Journal of Rock Mechanics and Geotechnical Engineering 14 (2022) 436–447

Contents lists available at ScienceDirect

Journal of Rock Mechanics and Geotechnical Engineering

journal homepage: www.jrmge.cn

Full Length Article

Assessing the deformation response of double-track overlapped tunnels using numerical simulation and field monitoring

Yao Hu [a,b], Huayang Lei [a,c,d,*], Gang Zheng [a,c,d,e], Liang Shi [a], Tianqi Zhang [a], Zhichao Shen [b], Rui Jia [a,c]

[a] School of Civil Engineering, Tianjin University, Tianjin, 300350, China
[b] Department of Civil and Environmental Engineering, National University of Singapore, 117576, Singapore
[c] Key Laboratory of Coast Civil Structure Safety (Tianjin University), Ministry of Education, Tianjin, 300350, China
[d] Key Laboratory of Earthquake Engineering Simulation and Seismic Resilience of China Earthquake Administration (Tianjin University), Tianjin, 300350, China
[e] State Key Laboratory of Hydraulic Engineering Simulation and Safety (Tianjin University), Tianjin, 300350, China

ARTICLE INFO

Article history:
Received 23 December 2020
Received in revised form
8 June 2021
Accepted 17 July 2021
Available online 28 August 2021

Keywords:
Double-track overlapped tunnels
Deformation response
Finite element analysis (FEA)
Field monitoring
Upper and lower tunneling

ABSTRACT

The unprecedented rate of metro construction has led to a highly complex network of metro lines. Tunnels are being overlapped to an ever-increasing degree. This paper investigates the deformation response of double-track overlapped tunnels in Tianjin, China using finite element analysis (FEA) and field monitoring, considering the attributes of different tunneling forms. With respect to the upper tunneling, the results of the FEA and field monitoring showed that the maximum vertical displacements of the ground surface during the tail passage were 2.06 mm, 2.25 mm and 2.39 mm obtained by the FEA, field monitoring and Peck calculation, respectively; the heaves on the vertical displacement curve were observed at 8 m (1.25*D*, where *D* is the diameter of the tunnel) away from the center of the tunnel and the curve at both sides was asymmetrical. Furthermore, the crown and bottom produce approximately 0.38 mm and 1.26 mm of contraction, respectively. The results of the FEA of the upper and lower sections demonstrated that the tunneling form has an obvious influence on the deformation response of the double-track overlapped tunnel. Compared with the upper tunneling, the lower tunneling exerted significantly less influence on the deformation response, which manifested as a smaller displacement of the strata and deformation of the existing tunnel. The results of this study on overlapped tunnels can provide a reference for similar projects in the future.

1. Introduction

The unprecedented rate of metro construction has become a highly complex network of metro lines. Overlapped tunnels have progressively appeared and become ever more intensive. Examples of overlapped tunnels include Beijing Metro Lines 2 and 4 between Beijing and Xuanwumen stations in China, the double-track overlapped tunnels of the MRT North-East Line in Singapore, the tunnel of Shenzhen Metro Shekou Line crossing right under the tunnel of Luobao Line in China, and the four-track overlapped tunnels between Xujiahui and Stadium stations of Shanghai Metro Lines 11 and 4 in China. In general, the environment surrounding overlapped tunnels tends to be complex and tunnel construction can cause a great ground disturbance, thus endangering the safety of adjacent building structures. Therefore, it is necessary to understand the deformation response induced by overlapped tunneling.

The geometric arrangement of overlapped tunnels has a significant effect on the deformation response during the tunneling process (Chehade and Shahrour, 2008; Shahin et al., 2016; Jin et al., 2019). Many studies have investigated the deformation response of overlapped tunnels with different geometric arrangements. For double-track overlapped tunnels, most research has focused on three types of geometric arrangements: horizontally parallel (Suwansawa and Einstein, 2007; Chen et al., 2011; Das et al., 2017; Zhang et al., 2019), vertically parallel (Ng et al., 2015; Fang et al., 2016), and intersecting (Marshall et al., 2013; Chen et al., 2018; Qian et al., 2019; Lai et al., 2020). Many studies have focused on

* Corresponding author. School of Civil Engineering, Tianjin University, Tianjin, 300350, China.
E-mail address: leihuayang74@163.com (H. Lei).
Peer review under responsibility of Institute of Rock and Soil Mechanics, Chinese Academy of Sciences.

https://doi.org/10.1016/j.jrmge.2021.07.003

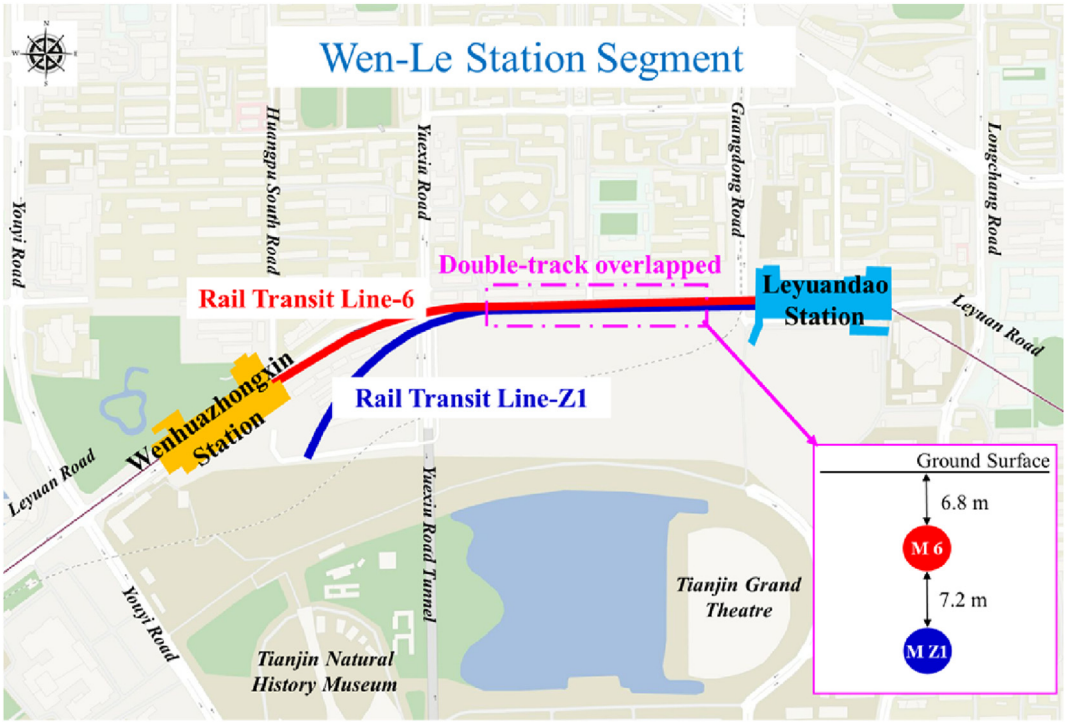

Fig. 1. Overview of the project: (a) location of M6 and (b) section of the double-track overlapped tunnel (Google Maps, annotations made by author).

horizontally parallel and intersecting arrangements, while few have focused on vertically parallel arrangements.

Among the studies that did consider vertically parallel double-track overlapped tunnels, Ng et al. (2015) used centrifuge tests and numerical modeling to analyze the deformation response during tunneling with a focus on the response of a pile group. Fang et al. (2016) investigated the ground surface settlement due to the tunneling process and considered the influence of different geometric arrangements; however, the tunnel section had a horseshoe shape and the shallow tunneling method was used for excavation. Few studies have considered the deformation response of vertically parallel double-track overlapped tunnels excavated by the shield tunneling method and with a circular tunnel section.

The tunneling form also affects the deformation response of double-track overlapped tunnels during the tunneling process. Ma et al. (2018) studied a pipeline's settlement and load-transfer mechanism induced by double-track overlapped tunneling with different tunneling forms. Soomro et al. (2020) employed centrifuge tests and numerical modeling to explore the stress-transfer mechanisms and settlement of a pile group during double-track overlapped tunneling with different construction sequences. However, the above studies focused on the response of existing pile groups and pipelines but did not evaluate the deformation response of existing tunnels.

In this study, finite element analysis (FEA) and field monitoring were employed to investigate the deformation response on the ground surface and new tunnel (longitudinal and transverse) during upper tunneling activity for the double-track overlapped tunnels in Tianjin, China. Moreover, the FEA of the upper and lower tunneling was used to explore the influence of the tunneling form on the deformation response of the double-track overlapped tunnels. The displacement in the strata (vertical and horizontal) and deformation of the existing tunnel (longitudinal and transverse) were analyzed in detail. The study of overlapped tunnels described in this paper can provide a reference for similar projects in the future.

2. Engineering background of the case study

2.1. Project overview

The section of double-track overlapped tunnels investigated belongs to the interval between Wenhuazhongxin and Leyuandao stations of Rail Transit Line 6 (M 6) in Tianjin, China. The total length of the interval between the two stations is 776 m and that of the double-track overlapped section of the tunnels is 392 m, as shown in Fig. 1.

An earth pressure balancing (EPB) shield machine with a diameter of 6.4 m was used to excavate the tunnel, and its face pressure was 0.25–0.3 MPa. The shield started from the working shaft of Wenhuazhongxin station and reached the working shaft of Leyuandao station. During the tunneling process, the shield passed the adjacent existing tunnels of Tianjin Rail Transit Line Z1 (M Z1) to form the section of the double-track overlapped tunnels. The tunnel lining was assembled with prefabricated reinforced concrete segments in staggered joints, which consisted of one cap block, two adjacent blocks, and three standard blocks. The strength grade of the segments is C55, and the segments are connected by bending bolts. In addition, the tunnel lining was designed to function with an outer diameter of 6.2 m and a thickness of 0.35 m, with the width of each ring being 1.5 m.

2.2. Geological conditions

Tianjin is located in the east of the North China Plain and downstream of the Haihe River Basin. It is an alluvial plain with flat terrain and extensive soft soil. Fig. 2 shows the illustration of the ground profile in the direction of the tunnel axis. It can be seen that the main strata of the interval between Wenhuazhongxin and Leyuandao stations consist of soft soils (including silty clay, sandy silt and silt), and the strata crossed by the double-track overlapped tunnels mainly consist of silty clay and silt. In addition, the minimum cover thickness of M 6 is 6.8 m, and the minimum vertical distance between M 6 and M Z1 is 7.2 m.

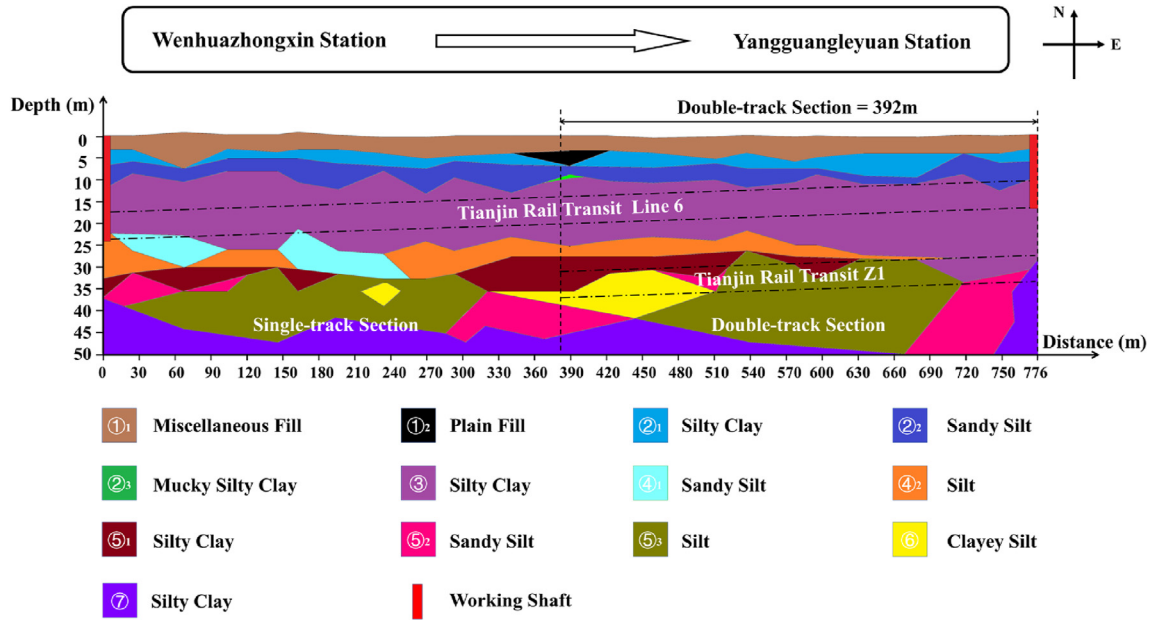

Fig. 2. Illustration of the ground profile in the direction of the tunnel axis.

Fig. 3 shows the variations of the typical geotechnical properties of the simplified soil layers with depth. These indices include unit weight, water content, void ratio, plasticity index, liquidity index, constrained factor, constrained modulus, cohesion, internal friction angle and standard penetration test (SPT) blow counts; and the minimum, maximum and average values of each index are given. During the construction process, the impact of unfavorable geological sections should be fully considered and the driving parameters should be properly set to avoid engineering risks. The groundwater table in the site is within the range of 0.8–1.9 m.

2.3. Field monitoring layout

Fig. 4 shows the field monitoring layout used in this study. The monitoring points were only arranged in the new tunnel (M 6) and on the ground surface to measure the deformation response of the double-track overlapped tunnels to the upper tunneling process, with a total of 5 monitoring points for vertical displacement of the ground surface, 18 monitoring points for longitudinal deformations of the tunnel, and 36 monitoring points for transverse deformations of the tunnel. Fig. 4a shows the top view of the field monitoring layout, and section *A*-*A*′ in the transverse direction was chosen to show the field monitoring layout of the new tunnel, as shown in Fig. 4b. "GS", "LS" and "TS" represent the monitoring points of vertical displacement on the ground surface, the longitudinal deformation of the tunnel, and the transverse deformation of the tunnel, respectively. The automatic leveling level DS05 (Suzhou FOIF Co., Ltd., China), the total station SET1X and prisms (Sokkia Co., Tokyo, Japan) and the hand-held laser rangefinder DLE50 (Robert Bosch GmbH, Stuttgart, Germany) were used in this study.

3. FEA of the double-track overlapped tunneling process

3.1. Finite element model

Given the engineering background of the double-track overlapped tunnels (upper tunneling), the three-dimensional FEA software, ABAQUS, was used to numerically explore the disturbance effect of the tunneling process on the double-track overlapped tunnels (Sun, 2015; Zhang et al., 2016). This paper chooses the small-strain FEA in the "Soils" step to calculate the deformation of soil, which can improve the computational efficiency (Liu et al., 2014).

When taking into account factors such as the burial depth and spacing of the two tunnels, it is generally appropriate to select a calculation range that is not less than 3*D*–4*D* along the tunnel diameter in all directions, where *D* is the diameter of the tunnel (Sun, 2015). Therefore, the dimensions of the finite element model were determined to be 63 m × 40 m × 46 m (length × width × depth), as shown in Fig. 5. The finite element model includes five types of components (soil part, shield part, grouting part, lining part, and an existing tunnel part) and two pressure types (support pressure of the shield tunneling face and grouting pressure); the dimensions of the parts and pressures are consistent with the actual project.

In this study, the C3D8P elements (8-node trilinear displacement and pore pressure) were selected to simulate soil strata because the pore water pressure must be considered. A non-uniform grid was used with a fine grid in the region close to the tunnel and a coarser grid in the far field. The C3D8I elements (8-node linear brick, incompatible mode) were employed to simulate the shield, grouting, lining, and existing tunnels (Dong et al., 2014). The finite element model has a total of 26,688 elements. Among these, the dualistic interactions between the soil and grouting parts, the soil and shield parts, the grouting and lining parts, and the soil and existing tunnel parts were connected by the tie. In addition, the boundary conditions of the model along the *X* and *Y* axes separately limited "U1" and "U2" to ensure that the horizontal displacement was constrained, whereas the vertical direction could be spontaneously moved. In the *Z* direction, "U1", "U2" and "U3" on the base surface were limited (both the horizontal and vertical directions are constrained).

Based on the upper tunneling activity, the finite element model of the lower tunneling (the existing tunnel is above and the new tunnel is below) is proposed as a basis for the discussion of the influence of the tunneling form on the deformation response of the

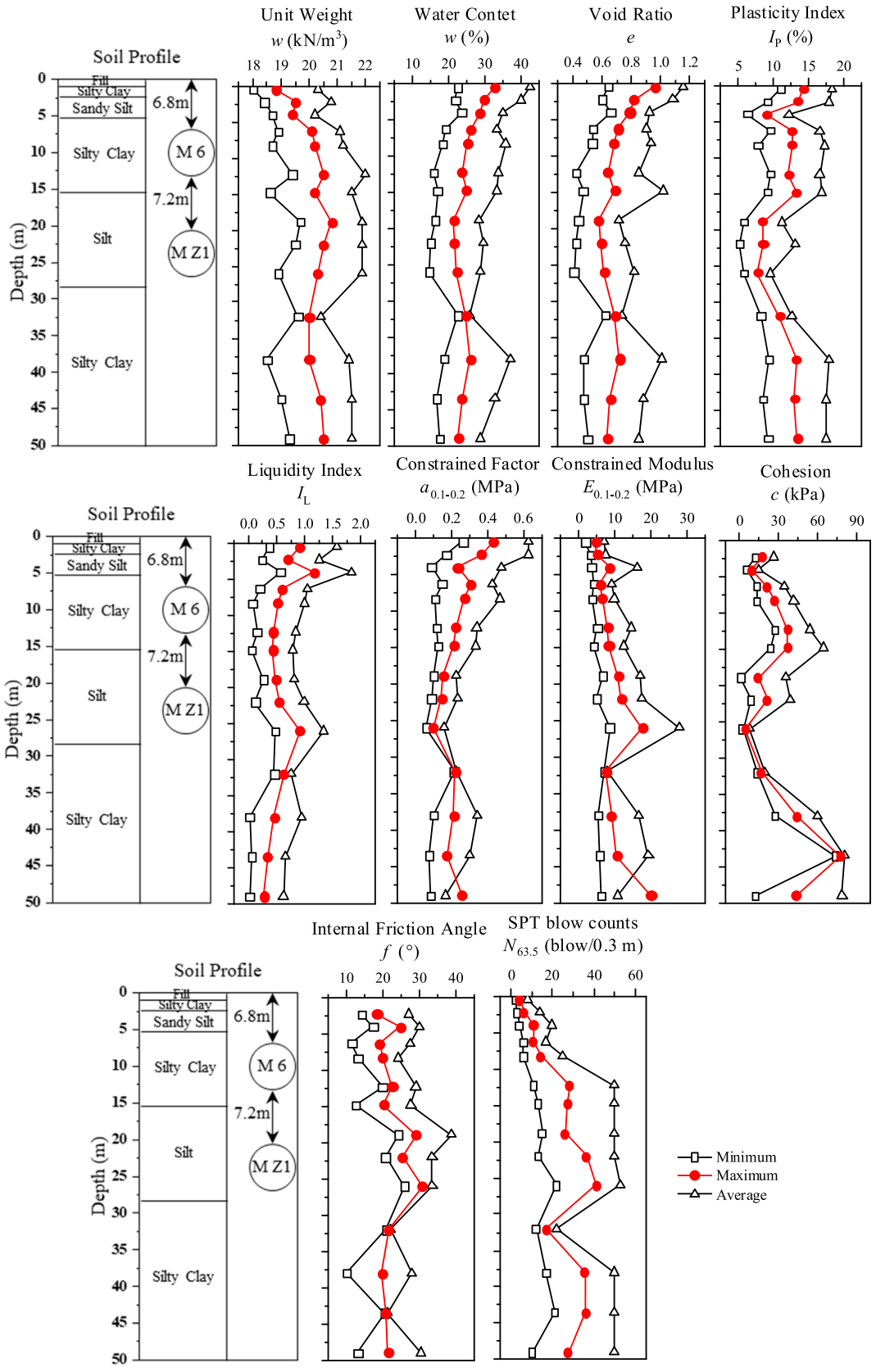

Fig. 3. Typical geotechnical properties and indices with depth.

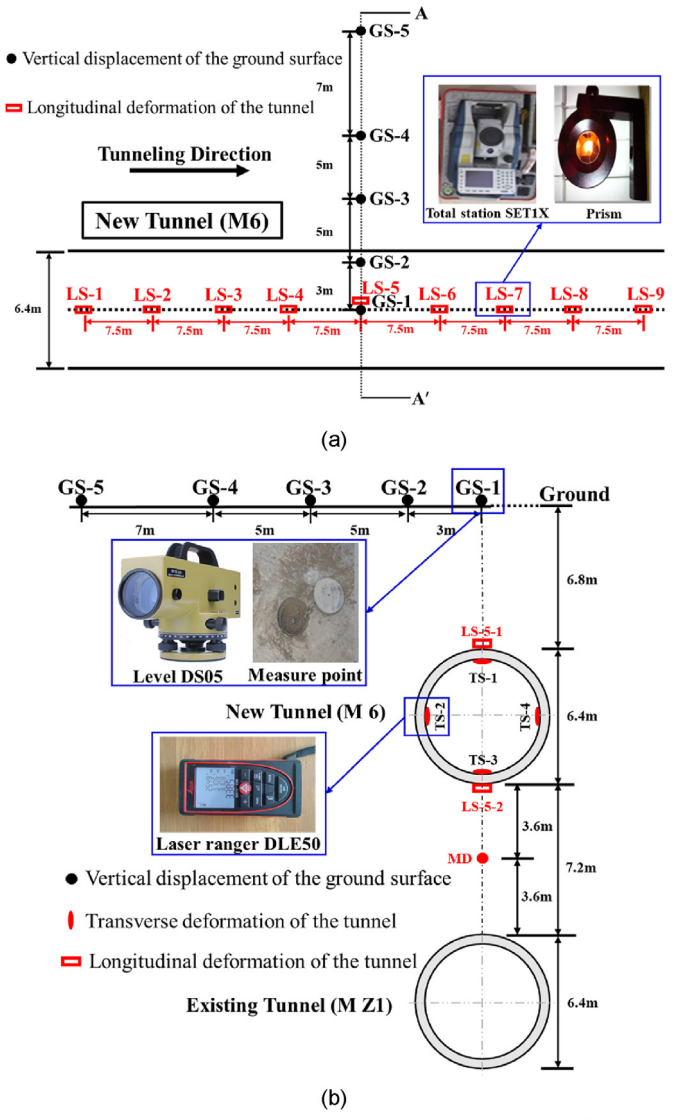

Fig. 4. Field-monitoring layout: (a) top view and (b) section A–A.

double-track overlapped tunnels. In the finite element model in the lower tunneling process, everything apart from the tunneling form is the same as that in the upper tunneling case.

3.2. Material properties

The material properties in this finite element model can be divided into two categories: elastoplastic material (soil) and linear elastic material (shield, lining, grouting, and the existing tunnel). For the soil, the elastic part adopts the porous elastic model, whereas the plastic part adopts the modified Cam-Clay model. As the materials are relatively uniform and have a high degree of stiffness, linear elastic constitutive models were used for the shield, lining, grouting, and existing tunnel (Zhang et al., 2016). The material parameters of the constitutive model used in the FEA are listed in Table 1. The finite element model considers the grouting hardening process, "soft" indicating that the grouting has just been injected and "hard" indicating that it has hardened. Furthermore, owing to the fact that the bolted connection between the linings in the actual project reduces its strength (Zheng et al., 2015; Zhang et al., 2021), the Young's modulus of the linings was discounted by 15% in this study (Sun, 2015). The parameters cannot be measured for the fill, and thus silty clay was used instead.

3.3. Modeling procedure

The shield construction process is complicated, involving shield tunneling, soil excavation, assembling lining, and shield tail grouting. In this study, this complex process was reasonably simplified using a "step-by-step tunneling" method (Mollon et al., 2013). In particular, the "element death" method was adopted to incorporate the tunneling process of the EPB shield machine, i.e. to create the "interaction" of "mode change" in ABAQUS. Fig. 6 introduces the detailed modeling procedure, which is described as follows:

(1) Initial earth stress balance: The acceleration due to gravity applied to the model (deactivation of the shield, grouting, and lining) is taken as 9.8 m/s^2 and then automatically balanced; the termination condition is that the displacement of the model is less than 1×10^{-6} m.
(2) Excavation 1: Reactivate the first slice shield (shield machine length: 10.5 m, which is equivalent to seven slices of lining), deactivate the first slice soil, and add the first support pressure from the shield tunneling face.
(3) Excavation 2: Reactivate the second slice shield (simultaneously deactivate the first slice shield), deactivate the second slice soil, add the second support pressure of the shield tunneling face (simultaneously remove the first support pressure), reactivate the first slice lining (simultaneously add the first slice grouting pressure), and reactivate the first slice soft-grouting.
(4) Excavation 3: Reactivate the third slice shield (simultaneously deactivate the second slice shield), deactivate the third slice soil, add the third support pressure of the shield tunneling face (simultaneously remove the second support pressure), reactivate the second slice lining (simultaneously add the second slice grouting pressure), and reactivate the second slice soft-grouting (simultaneously hardening the first slice grouting).
(5) Repeat Steps (2)–(4) until the shield has been moved out of the hole.

4. Results and discussion

FEA and field monitoring results were compared to investigate the deformation response of the double-track overlapped tunnels during the upper tunneling process. The following aspects were primarily analyzed: (1) vertical displacement of GS-1 during different tunneling stages, (2) vertical displacement of the ground surface, (3) longitudinal deformation of the new tunnel, and (4) transverse deformation of the new tunnel. Based on this, the influence of different tunneling forms on the double-track overlapped tunnels was evaluated via an FEA of the upper and lower tunneling.

4.1. Vertical displacement of GS-1 during different tunneling stages

Fig. 7 shows the vertical displacement of the ground surface at monitoring point GS-1 during different tunneling stages. Before GS-1 was reached (face pre-arrival), the heave occurred, which was observed in both the FEA and field monitoring. Liu et al. (2014) stated that the face pressure (i.e. the pressure of earth acting on the tunnel face) is the main influencing factor before the tunnel face is reached during the tunneling process. Therefore, it can be deduced that this heave was primarily caused by face pressure.

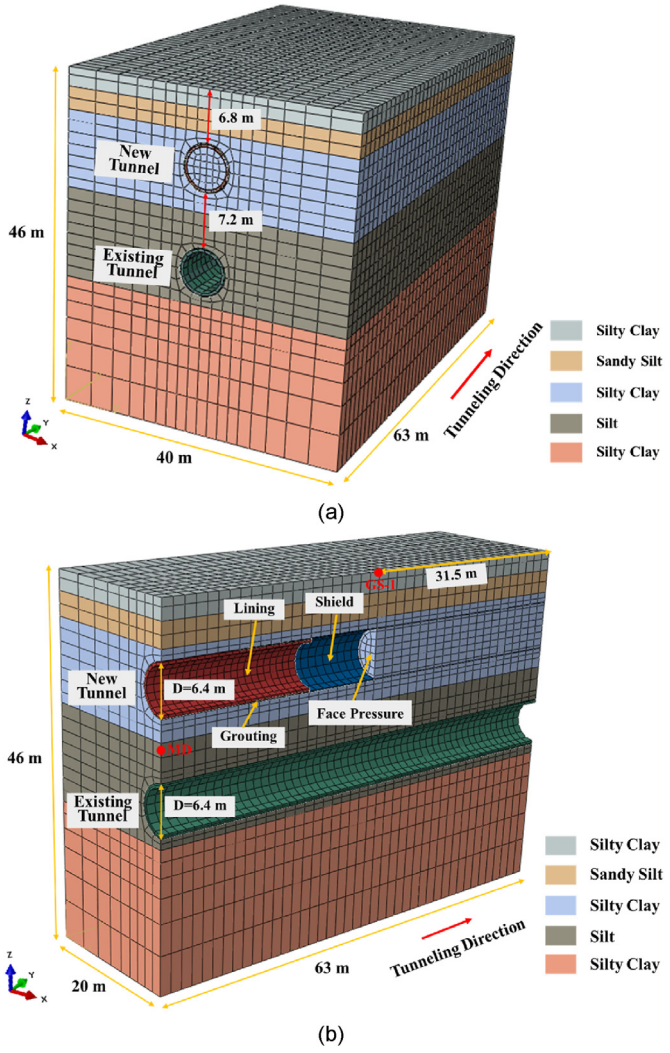

Fig. 5. Finite element model meshing of the upper tunneling: (a) whole view and (b) cut in half along the Y-axis.

When GS-1 was crossed (face arrival), the settlement was observed by both approaches, but the field monitoring revealed greater settlement than FEA did. According to Ji et al. (2008), at this stage, the conicity of the shield machine (Fig. 8a) and ovalization of the lining (Fig. 12) may have the greatest influence on the vertical displacement. After GS-1 was passed (tail passage), the settlement was still revealed by the two approaches, but the difference between field monitoring and FEA was greater than that for the face arrival. The settlement at this stage may be attributed to the grouting pressure and contraction during grouting.

In this study, the conicity of the shield machine was considered in the field monitoring but not in the FEA. In addition, the field monitoring indicated non-uniform contraction during grouting (Fig. 8b), whereas the FEA revealed uniform contraction. These explain the differences between field monitoring and FEA. Compared with the maximum vertical displacements observed for a single tunnel (FEA: 20 mm; field monitoring: 7.5 mm) (Liu et al., 2014), the maximum vertical displacements in this study were significantly smaller (FEA: 2.5 mm; field monitoring: 1.5 mm). This may be attributed to the effect of the existing tunnel.

4.2. Vertical displacement of the ground surface

To further explore the response to the tunnel construction, the Peck (1969) formula was used to calculate the transverse vertical displacement of the ground surface in the tunneling process. Based on the geological conditions of this case, Eq. (1) was used to calculate the width of the settlement trough i (Wei, 2009):

$$i = m\left[R + h\tan\left(45^\circ - \frac{\varphi}{2}\right)\right] \tag{1}$$

where m is a coefficient in the range of 0.45–0.5, R is the tunnel radius, h is the depth of the tunnel axis, and φ is the internal friction angle of the soil above the tunnel.

Fig. 9 compares the transverse vertical displacement of the ground surface in the tunneling process (i.e. excavated to a distance of 31.5 m) for the FEA with the field monitoring and Peck calculation. Fig. 9a presents the tunneling face arrival stage, while Fig. 9b shows the shield tail passage stage. It can be seen that except for the maximum vertical displacement, the trend of the vertical displacement from the center of the tunnel to the two sides is similar for the face arrival and tail passage stages. The maximum vertical displacement during the tail passage (FEA: 2.06 mm) is significantly greater than that of the face arrival (FEA: 1.02 mm). Therefore, we take the tail passage (Fig. 9b) as an example for analysis.

As shown in Fig. 9b, the trend of the vertical displacement obtained by the FEA is similar to both the field monitoring and Peck calculation, all of which have a settlement trough. Compared with the field monitoring (2.25 mm) and Peck calculation (2.39 mm), FEA (2.06 mm) tends to provide a smaller maximum vertical displacement under the tail passage stage. This may be because the conicity of the shield machine and non-uniform contraction during grouting are not taken into account in the FEA (Fig. 8). Furthermore,

Table 1
Material constitutive parameters used in the finite element analysis.

Soil layers	Thickness (m)	Unit weight (kN/m^3)	M	λ	κ	ν	k (m/d)	e_0
Silty Clay	2.5	18.4	0.86	0.058	0.0072	0.32	0.00018	0.776
Sandy Silt	3	17.9	1.03	0.031	0.0039	0.35	0.00050	0.742
Silty Clay	10.3	18.1	0.89	0.055	0.0069	0.35	0.00031	0.764
Silt	12.2	19.8	1.37	0.020	0.0025	0.3	0.00020	0.595
Silty Clay	18	18.6	0.90	0.047	0.0059	0.35	0.00485	0.683

Materials		Thickness (m)	Unit weight (kN/m^3)	E (MPa)	ν
Existing tunnel		0.45	20	2×10^4	0.3
Shield		0.1	78	2.4×10^5	0.2
Grouting	Soft	0.1	20	5	0.4
	Hard			18	0.2
Lining		0.35	25	2.93×10^4 (15% discount)	0.2

Note: E: Young's modulus; ν: Poisson's ratio; M: Slope of the critical state line in q–p' space; λ and κ: Slopes of the normal compression and recompression lines in e–ln p' space; e_0: Initial void ratio; k: Permeability coefficient.

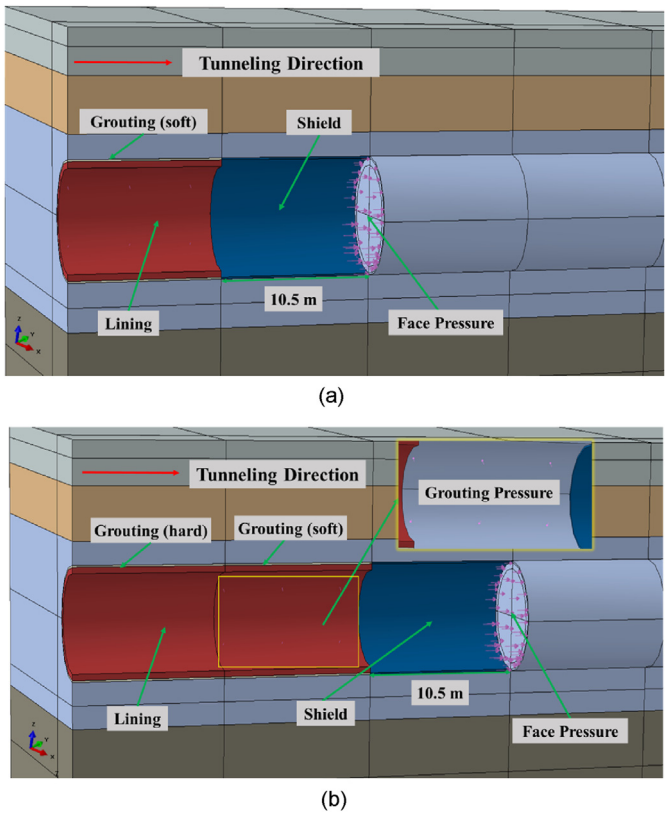

Fig. 6. Finite element modeling procedure of the double-track overlapped tunnel: (a) excavation 2 and (b) excavation 3.

in the FEA and field monitoring, the vertical displacement curve is uplifted at 8 m (1.25D) away from the center of the tunnel, but this is not seen in the Peck calculation. The reason for this heave is the upward movement of the existing tunnel due to buoyancy (Zheng et al., 2019), which requires that the release of water pressure during metro tunnel construction should be regulated.

Zheng et al. (2019) conducted field monitoring on the overlapped tunnel to study the vertical displacement of the ground surface. The construction sequence was as follows: the down-line tunneling followed by the up-line tunneling one year later. Fig. 10 shows a comparison of the results between Zheng et al. (2019) and this study during the tail passage. Clearly, the four trends of the vertical displacement are similar, with a heave on the vertical displacement curve at the left and right sides of the tunnel (in this study, field monitoring is only performed on the left of the tunnel). In addition, apart from the field monitoring in this study, the vertical displacements on the left and right sides of the tunnel are asymmetrical and their uplift values are different.

4.3. Longitudinal deformation of the new tunnel

Fig. 11 indicates the longitudinal deformation of the new tunnel after tunneling (i.e. excavated to a distance of 63 m) in the FEA and field monitoring. The deformation ΔD can be calculated from the difference in the longitudinal deformation between the bottom and crown after tunneling:

$$\Delta D = \frac{D_{\text{bottom}} - D_{\text{crown}}}{2} \tag{2}$$

where D_{bottom} and D_{crown} are the longitudinal deformations of the tunnel at the bottom and crown, respectively. The positive values at the crown and bottom of the tunnel mean that they underwent expansion and contraction, respectively. Furthermore, the positive value of the difference between the bottom and crown means that the tunnel collectively moved upward.

It can be seen from Fig. 11 that the longitudinal deformation trends of the FEA and field monitoring after tunneling are almost identical. The trend can be divided into three stages: Stage I: the longitudinal deformation increases and reaches the maximum (positive) at 42.5 m (3.2D) away from the end of tunnel; Stage II: the longitudinal deformation drops sharply and reaches the minimum (negative) at 56.5 m (1D) away from the end of tunnel; and Stage III: the longitudinal deformation has a slight increase. This indicates that the tunnel deformation changed from upward movement to downward movement at 1D–3.2D away from the end of the tunnel. Attention should be given to the tunnel deformation at 3.2D away from the end of the tunnel for the construction of double-track overlapped tunnels. The difference between the FEA and field monitoring may be attributed to the difference in connections between the linings. In other words, the FEA adopted the equivalent stiffness method, while bolted connections were used in the actual engineering project.

4.4. Transverse deformation of the new tunnel

Fig. 12 shows the transverse deformation of the new tunnel in the upper tunneling process. The transverse deformations obtained by the FEA and field monitoring are essentially the same. Compared with the pre- and post-tunneling stages, the left and right sides of the new tunnel produce a non-uniform expansion (0.68 mm at the left and 0.49 mm at the right), whereas the crown and bottom produce 0.38 mm and 1.26 mm of contraction, respectively. Clearly, there is a greater deformation at the bottom of the tunnel than at the crown. The reasons for this are the excavation of soil causing a stress release and the thin overburden of the soil (6.8 m $\approx$ 1.06D), which lead to the center of the new tunnel moving upwards after tunneling compared with the case prior to tunneling. This also explains the heave of ground surface at both sides of the tunnel described in Section 4.2 (Fig. 9).

4.5. Influence of tunneling form on the deformation response

A comparison of the FEA results between upper and lower tunneling was performed to discuss the influence of the tunneling form on the deformation response of the double-track overlapped tunnels. The following aspects were analyzed: (1) vertical displacement of the strata, (2) horizontal displacement of the strata, (3) longitudinal deformation of the existing tunnel, and (4) transverse deformation of the existing tunnel.

4.5.1. Vertical displacement of the strata

Fig. 13 shows the vertical displacement of the ground surface and monitoring point MD (between the new and existing tunnel, at a depth of 16.8 m) in accordance with different tunneling forms. Fig. 13a shows the longitudinal direction after tunneling. On the ground surface, the vertical displacement due to different tunneling forms (upper and lower) gradually increases with tunneling. However, the increase is relatively large in the upper tunneling process and its value ranges from −0.66 mm to −2.78 mm, whereas the increased range is relatively small during the lower tunneling and its value ranges from −0.66 mm to −1.11 mm. The difference between the upper and lower tunneling is 0 mm and 1.67 mm at 0 m and 63 m away from the starting position of tunneling, respectively. At the monitoring point MD, the vertical displacement fluctuates by 3 mm in the upper tunneling process, but it increases with small fluctuations arising

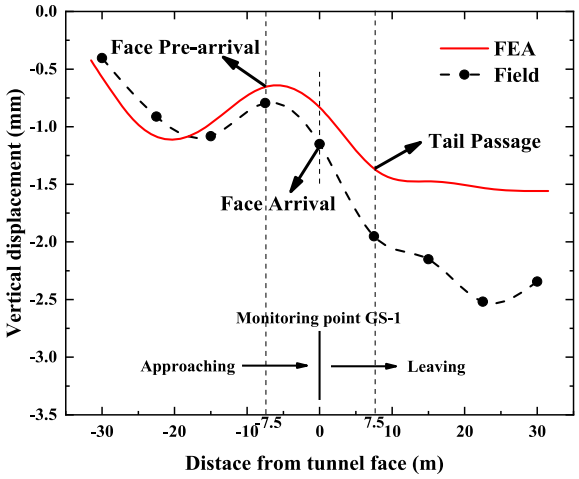

Fig. 7. Vertical displacement of monitoring point GS-1 during different tunneling stages.

from lower tunneling and its value ranges from −0.39 mm to −1.02 mm. The difference between the upper and lower tunneling is 3.41 mm and 3.99 mm at 0 m and 63 m away from the starting position of tunneling, respectively.

Fig. 13b shows the transverse direction in the upper and lower tunneling processes (i.e. excavated to a distance of 31.5 m). On the ground surface, the trends of vertical displacement in the upper and lower tunneling processes are essentially the same, with both being settled. However, the settlement of the strata induced by the upper tunneling (maximum value of −2.06 mm) is obviously greater than that by the lower tunneling (maximum value of −0.37 mm). At the monitoring point MD, the trends of vertical displacement in accordance with two tunneling forms are reversed, i.e. the upper tunneling shows a heave (maximum value of 2.5 mm) and the lower tunneling shows a settlement (maximum value of −0.11 mm).

The above analysis shows that the effects of different tunneling forms on the vertical displacement of the strata are completely different. The upper tunneling causes the strata to settle on the ground surface and to heave at the monitoring point MD, whereas the lower tunneling has little influence on the ground surface and induces settlement in the monitoring point MD. This indicates that during lower tunneling activity, the existing tunnel has an inhibitory effect on the vertical displacement of the ground surface.

4.5.2. Horizontal displacement of the strata

Fig. 14 illustrates the transverse horizontal displacement of the strata in the upper and lower tunneling processes under different tunneling forms and at different stages. The trends of the transverse horizontal displacement at two stages (face arrival and tail passage) are similar, and the difference in the magnitude, i.e. the horizontal displacement value of the tail passage, is greater than that during the face arrival. Thus, only the tail passage was selected for analysis in this study.

The result of the tail passage indicates that under upper and lower tunneling, the differences among the horizontal displacement-depth responses mainly occur at the location of the new tunnel (upper tunneling at a depth of 10 m and lower tunneling at a depth of 23.6 m). Compared with the lower tunneling (1.44 mm), the maximum value of the horizontal displacement during upper tunneling (2.63 mm) is larger. According to previous research, the cover thickness of a new tunnel (Zhang et al., 2016), ovalization of the tunnel lining (Liu et al., 2014), and geometric arrangement between overlapped tunnels (Fang et al., 2016) are critical factors influencing the horizontal displacement of the strata during the tunneling process. We can infer that this difference between the maximum horizontal displacements in the upper and lower tunneling processes can be attributed to the factors such as the buried depth of the new tunnel, its deformation, and the position of the existing tunnel.

The direction of horizontal displacement was outward from the tunnel, which is consistent with the results of Dias and Kastner (2013). However, this can change depending on the situation. For example, Zhang et al. (2016) observed inward movement, and Standing and Selemetas (2013) observed both inward and outward movements. The direction of horizontal displacement may be related to the new tunnel deformation. In this study, the expansion on both sides of the new tunnel (Fig. 12) led to an outward movement. Furthermore, the position of the maximum horizontal displacement has a slight upward deviation from the original position of the tunnel's center and that upward shift is greater during upper tunneling activity. This was due to the discrepancy in the cover thickness of the new tunnel. The lower tunnel had a cover thickness of 20.4 m, while the upper tunnel had a cover thickness of only 6.8 m.

4.5.3. Longitudinal deformation of the existing tunnel

Fig. 15 shows the longitudinal deformation of the existing tunnel after upper and lower tunneling. Upward deformation is defined as positive, whereas downward deformation is defined as negative. In the upper tunneling process, the variations of the longitudinal deformation at the crown and bottom are roughly the same, but the longitudinal deformation of the former is significantly larger than that of the latter. The deformation values range from 2.26 mm to 2.38 mm at the crown and from 1.56 mm to 1.67 mm at the bottom. In the lower tunneling process, the variations of the longitudinal deformation at the crown and bottom are essentially the same, with a difference of only 0.05 mm. In addition, compared with the upper tunneling process, the longitudinal deformation and difference between the crown and bottom in the lower tunneling process are significantly smaller. The longitudinal deformation of the existing tunnel is caused by the strata displacement, especially the vertical displacement. This is consistent with the large difference between the two tunneling forms in terms of the vertical displacement of the strata.

4.5.4. Transverse deformation of the existing tunnel

Fig. 16 shows the transverse deformation of the existing tunnel in the upper and lower tunneling processes. The deformation of the existing tunnel in the transverse direction is more intuitive. In the upper tunneling process, compared with pre- and post-tunneling, the left and right sides of the existing tunnel present a contraction of approximately 1.56 mm, whereas the crown and bottom have upward deformations of about 1.78 mm and 1.49 mm, respectively. This indicates that the existing tunnel collectively moves up. The reason for this is that the stress release caused by the excavation of the new tunnel results in the upward displacement of the strata, thus affecting the existing tunnel. In the lower tunneling process, the deformation of the existing tunnel prior to and after tunneling is very small, i.e. only 0.25 mm. Therefore, compared with upper tunneling, the transverse deformation of the existing tunnel in the lower tunneling process is significantly smaller. This also explains the upward deviation of the position of the maximum horizontal displacement described in Section 4.5.2 (Fig. 14). Clearly, the tunneling form has a great influence on the deformation response of the existing tunnel.

The above analysis shows that compared with the lower tunneling, the upper tunneling had a greater influence on the

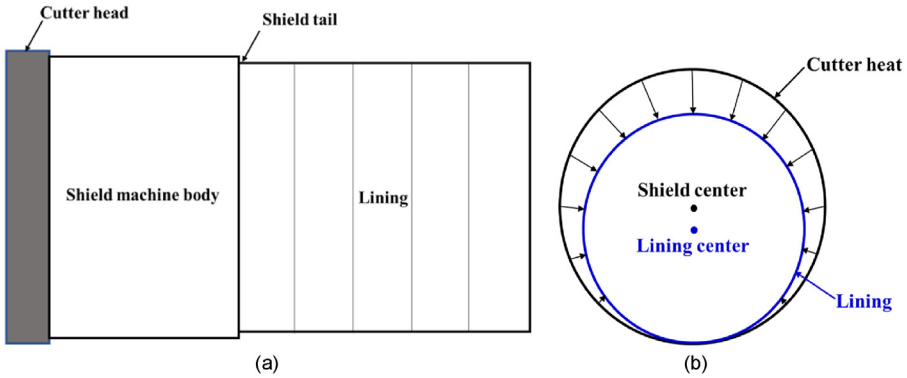

Fig. 8. Influence factors: (a) conicity of the shield machine and (b) nonuniform contraction.

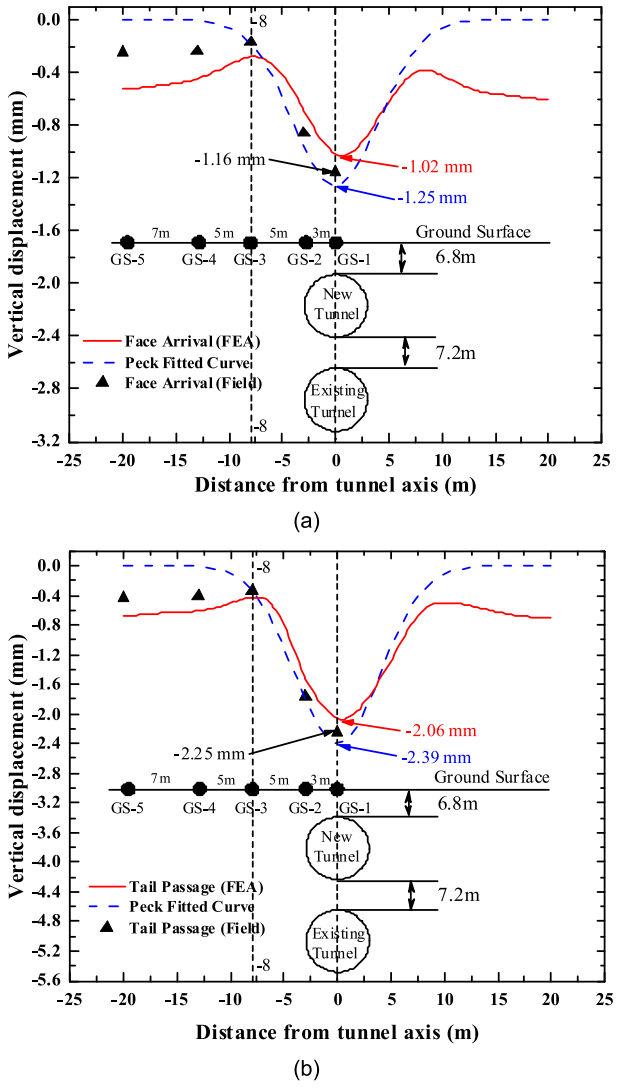

Fig. 9. Transverse vertical displacement of the ground surface in the middle of the tunnel: (a) Face arrival, and (b) Tail passage.

deformation response of the double-track overlapped tunnels. This manifested as a greater displacement of the strata and deformation of the existing tunnel. This may be because there was no existing tunnel on the top during the upper tunneling and the cover thickness was very small (6.4 m ≈ 1.06*D*). By contrast, there was an existing tunnel on the top during the lower tunneling, which inhibited the deformation response of the strata and existing tunnel. Based on this, some suggestions for similar engineering projects in the future are given. Compared with the lower tunneling, the upper tunneling should be given attention when the cover thickness is only about 1*D*. The strata should be reinforced in the vertical and horizontal directions to reduce the displacement. The left and right sides of the existing tunnel should be reinforced to mitigate the contraction, and its crown and bottom should be reinforced to reduce the upward deformation.

5. Conclusions

A case study was conducted on double-track overlapped tunnels in Tianjin, China using FEA and field monitoring to explore the deformation response during upper tunneling and the influence of the tunneling form. The main conclusions are drawn as follows:

(1) Similar results were obtained by FEA and field monitoring in this case study. The vertical displacement at the monitoring point GS-1 showed uplift before it was reached and settlement after it was passed. The Peck formula was used to calculate the vertical displacement of the ground surface; the maximum vertical displacements for tail passage (FEA: 2.06 mm, field monitoring: 2.25 mm, and Peck: 2.39 mm)

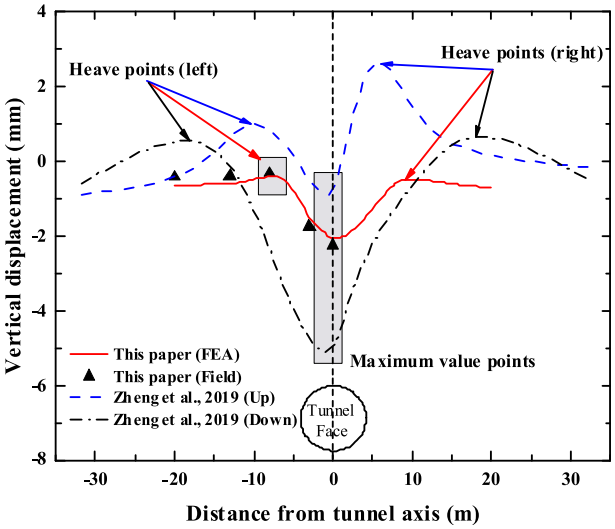

Fig. 10. Comparison of the results of Zheng et al. (2019) and this study for the tail passage state.

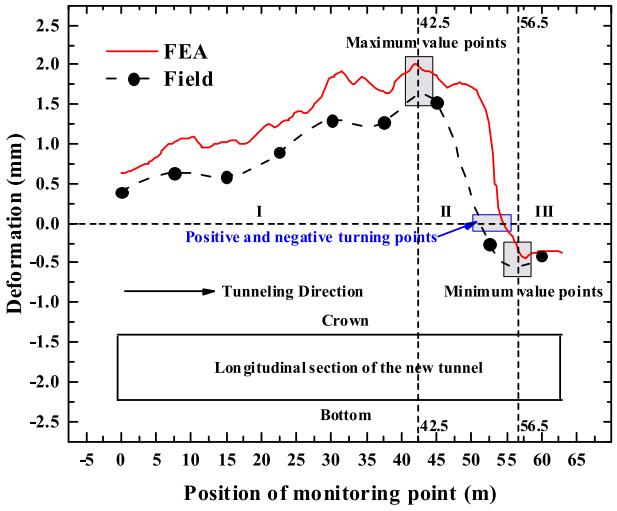

Fig. 11. Longitudinal deformation of the new tunnel after tunneling completion.

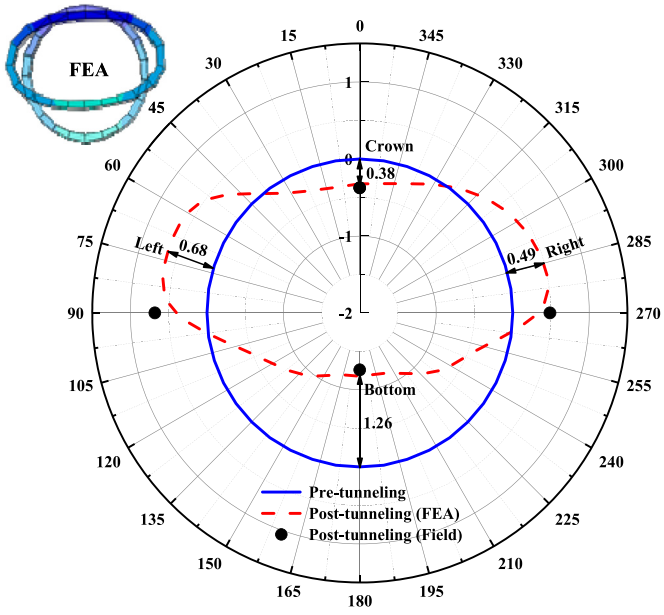

Fig. 12. Transverse deformation of the new tunnel in the middle of tunneling (unit: mm). The numbers around the circle are in degree.

were significantly greater than those for face arrival (FEA: 1.02 mm, field monitoring: 1.16 mm, and Peck: 1.25 mm). Furthermore, a heave on the vertical displacement curve was observed at 8 m (1.25*D*) away from the center of the tunnel, and the curve at both sides was asymmetrical. The results were compared for verification. The longitudinal deformation of the new tunnel changed from upward to downward between 1*D* and 3.2*D* from the end of the tunnel. The transverse deformation of the new tunnel showed expansion at the left (0.68 mm) and right (0.49 mm) sides, whereas an upward movement was generated at the center and contraction was produced at the crown (0.38 mm) and bottom (1.26 mm).

(2) FEA of the upper and lower tunneling was implemented to explore the influence of the tunneling form on the deformation response of the strata and existing tunnel. The tunneling form significantly influenced the deformation

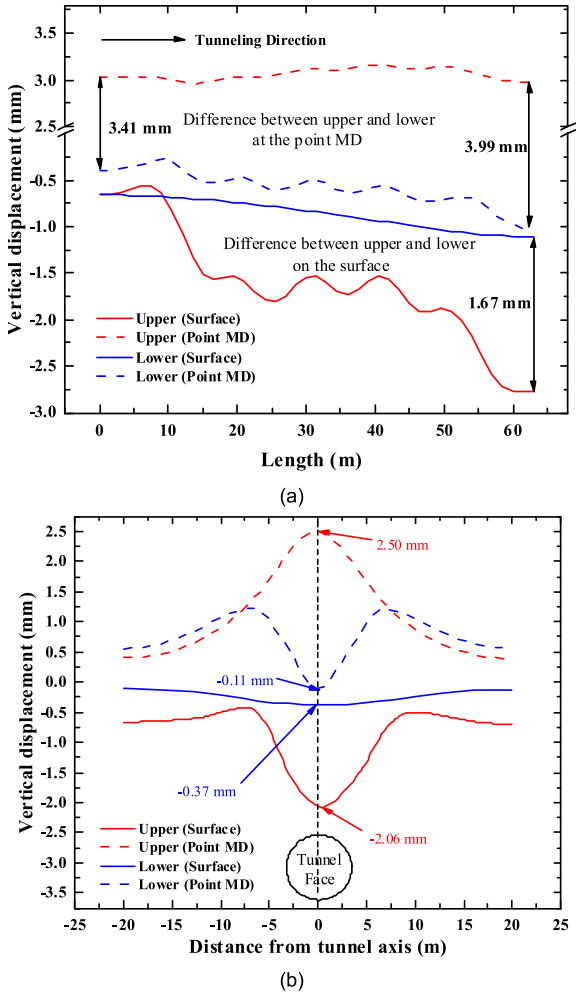

Fig. 13. Vertical displacement of the stratum: (a) longitudinal (after tunneling) and (b) transverse (in the middle of tunneling).

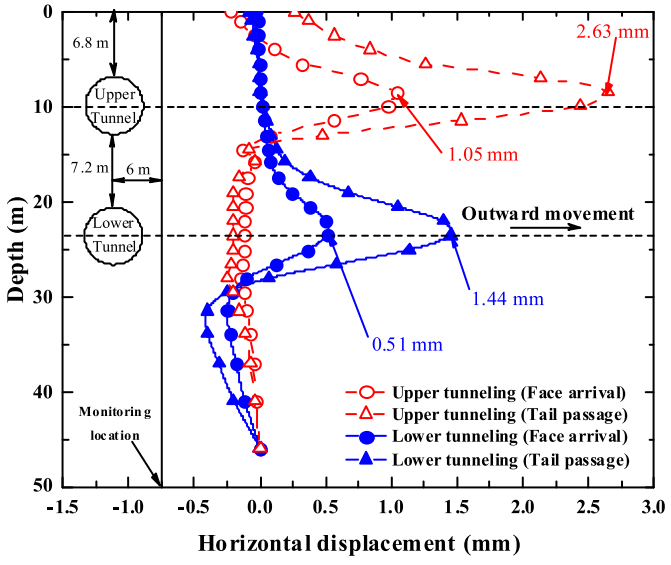

Fig. 14. Transverse horizontal displacement of the stratum in the middle of tunneling.

response during the tunneling of the double-track overlapped tunnels. Regarding the vertical displacement, the

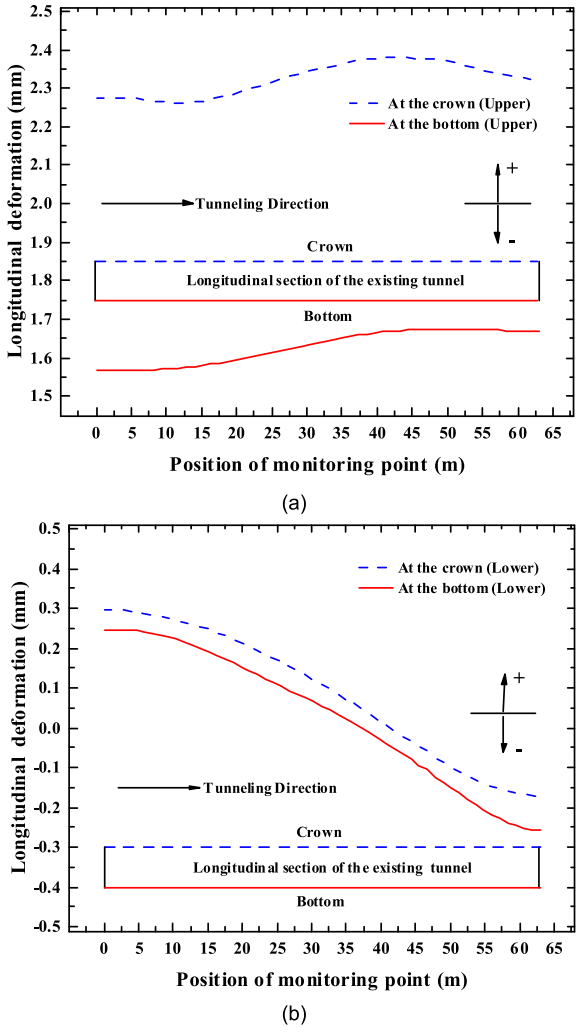

Fig. 15. Longitudinal deformation of the existing tunnel after tunneling: (a) upper tunneling; and (b) lower tunneling.

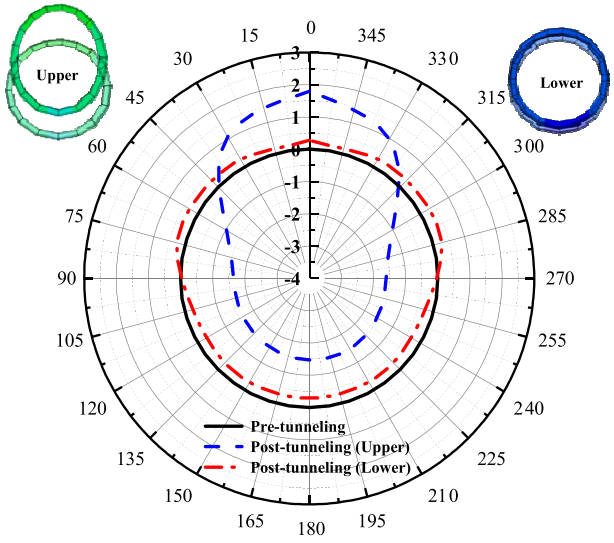

Fig. 16. Transverse deformation of the existing tunnel in the middle of tunneling (unit: mm). The numbers around the circle are in degree.

upper tunneling caused the strata to settle on the ground surface and to heave at the monitoring point MD, whereas the lower tunneling had little influence on the ground surface and induced settlement at the monitoring point MD. Regarding the horizontal displacement, the upper tunneling caused a greater maximum displacement (2.63 mm) than the lower tunneling (1.44 mm). In addition, the position of the maximum displacement deviated slightly upward from the original position at the tunnel center. For the existing tunnel, the longitudinal deformation and difference at the crown and bottom during the lower tunneling were significantly smaller than that during the upper tunneling. The lower tunneling had a significantly smaller transverse deformation (upward deformation of 0.25 mm) than the upper tunneling (1.56 mm contraction at the left and right sides, 1.78 mm upward deformation at the crown, and 1.49 mm upward deformation at the bottom).

Data availability statement

Some or all data, models, or code that support the findings of this study are available from the corresponding author upon reasonable request.

Declaration of competing interest

The authors declare that they have no known competing financial interests or personal relationships that could have appeared to influence the work reported in this paper.

Acknowledgments

The work described in this paper was financially supported by the Open Project of the State Key Laboratory of Disaster Reduction in Civil Engineering (Grant No. SLDRCE17-01), the National Key Research and Development Program of China (Grant No. 2017YFC0805402), and the National Natural Science Foundation of China (Grant No. 51808387). All the support is greatly appreciated.

References

Chehade, F.H., Shahrour, I., 2008. Numerical analysis of the interaction between twin-tunnels: influence of the relative position and construction procedure. Tunn. Undergr. Space Technol. 23 (2), 210–214.
Chen, R.P., Zhu, J., Liu, W., Tang, X.W., 2011. Ground movement induced by parallel EPB tunnels in silty soils. Tunn. Undergr. Space Technol. 26 (1), 163–171.
Chen, R.P., Lin, X.T., Kang, X., Zhong, Z.Q., Liu, Y., Zhang, P., Wu, H.N., 2018. Deformation and stress characteristics of existing twin tunnels induced by close-distance EPBS under-crossing. Tunn. Undergr. Space Technol. 82, 468–481.
Das, R., Singh, P.K., Kainthola, A., Panthee, S., Singh, T.N., 2017. Numerical analysis of surface subsidence in asymmetric parallel highway tunnels. J. Rock Mech. Geotech. Eng. 9 (1), 170–179.
Dias, D., Kastner, R., 2013. Movements caused by the excavation of tunnels using face pressurized shields - analysis of monitoring and numerical modeling results. Eng. Geol. 152 (1), 17–25.
Dong, Y., Burd, H., Houlsby, G., Hou, Y., 2014. Advanced finite element analysis of a complex deep excavation case history in Shanghai. Front. Struct. Civ. Eng. 8 (1), 93–100.
Fang, Q., Tai, Q., Zhang, D.L., Wong, L.N.Y., 2016. Ground surface settlements due to construction of closely-spaced twin tunnels with different geometric arrangements. Tunn. Undergr. Space Technol. 51, 144–151.
Ji, Q., Huang, Z., Peng, X., 2008. Analysis on influence of conicity of extra-large diameter mixed shield machine on surface settlement. In: Complimentary Special Issue to the 6th International Symposium on Geotechnical Aspects of Underground Construction in Soft Ground. Shanghai, China, pp. 237–242.
Jin, D., Yuan, D., Liu, S., Li, X., Luo, W., 2019. Performance of existing subway tunnels undercrossed by four closely spaced shield tunnels. J. Perform. Constr. Facil. 33 (1), 04018099.
Lai, H.P., Zheng, H.W., Chen, R., Kang, Z., Liu, Y., 2020. Settlement behaviors of existing tunnel caused by obliquely under-crossing shield tunneling in close proximity with small intersection angle. Tunn. Undergr. Space Technol. 97, 103258.

Liu, C., Zhang, Z.X., Regueiro, R.A., 2014. Pile and pile group response to tunnelling using a large diameter slurry shield – case study in. Shanghai. Comput. Geotech. 59, 21–43.
Ma, S., Liu, Y., Lv, X., Shao, Y., Feng, Y., 2018. Settlement and load transfer mechanism of pipeline due to twin stacked tunneling with different construction sequences. KSCE J. Civ. Eng. 22, 3810–3817.
Marshall, A.M., Klar, A., Mair, R.J., 2010. Tunneling beneath buried pipes: view of soil strain and its effect on pipeline behavior. J. Geotech. Geoenviron. 136 (12), 1664–1672.
Mollon, G., Dias, D., Soubra, A.H., 2013. Probabilistic analyses of tunneling-induced ground movements. Acta Geotechnol. 8 (2), 181–199.
Ng, C.W.W., Hong, Y., Soomro, M.A., 2015. Effects of piggyback twin tunnelling on a pile group: 3D centrifuge tests and numerical modelling. Geotechnique 65 (1), 38–51.
Peck, R.B., 1969. Deep excavations and tunneling in soft ground. In: Proceedings of the 7th International Conference on Soil Mechanics and Foundation Engineering. Mexico City, Mexico, pp. 225–290.
Qian, W.Q., Qi, T.Y., Zhao, Y.J., Le, Y.Z., Yi, H.Y., 2019. Deformation characteristics and safety assessment of a high-speed railway induced by undercutting metro tunnel excavation. J. Rock Mech. Geotech. Eng. 11 (1), 88–98.
Shahin, H.M., Nakai, T., Ishii, K., Iwata, T., Kuroi, S., 2016. Investigation of influence of tunneling on existing building and tunnel: model tests and numerical simulations. Acta Geotechnol. 11, 679–692.
Soomro, M.A., Mangi, N., Xiong, H., Kumar, M., Mangnejo, D.A., 2020. Centrifuge and numerical modelling of stress transfer mechanisms and settlement of pile group due to twin stacked tunnelling with different construction sequences. Comput. Geotech. 121, 103449.
Standing, J.R., Selemetas, D., 2013. Greenfield ground response to EPBM tunnelling in London Clay. Geotechnique 63 (12), 989–1007.
Suwansawa, S., Einstein, H.H., 2007. Describing settlement troughs over twin tunnels using a superposition technique. J. Geotech. Geoenviron. 133 (4), 445–468.
Sun, F.M., 2015. Analysis of Interaction between Small-Spacing Parallel Shield Tunnel Excavations. MSc Thesis. Zhejiang University, Hangzhou, China (in Chinese).
Wei, G., 2009. Study on calculation for width parameter of surface settlement trough induced by shield tunnel. Ind. Constr. 39 (12), 74–79 (in Chinese).
Zhang, T.Q., Taylor, R.N., Divall, S., Zheng, G., Sun, J., Stallebrass, S.E., Goodey, R.J., 2019. Explanation for twin tunnelling-induced surface settlements by changes in soil stiffness on account of stress history. Tunn. Undergr. Space Technol. 85, 160–169.
Zhang, Z.X., Liu, C., Huang, X., Kwok, C.Y., Teng, L., 2016. Three-dimensional finite-element analysis on ground responses during twin-tunnel construction using the URUP method. Tunn. Undergr. Space Technol. 58, 133–146.
Zhang, J.Z., Huang, H.W., Zhang, D.M., Zhou, M.L., Tang, C., Liu, D.J., 2021. Effect of ground surface surcharge on deformational performance of tunnel in spatially variable soil. Comput. Geotech. 136, 104229.
Zheng, G., Lu, P., Diao, Y., 2015. Advance speed-based parametric study of greenfield deformation induced by EPBM tunneling in soft ground. Comput. Geotech. 65, 220–232.
Zheng, G., Fan, Q., Zhang, T., Zheng, W., Sun, J., Zhou, H., Diao, Y., 2019. Multistage regulation strategy as a tool to control the vertical displacement of railway tracks placed over the building site of two overlapped shield tunnels. Tunn. Undergr. Space Technol. 83, 282–290.

Dr. Huayang Lei has obtained her BSc degree in Engineering Geology at College of Changchun Geology, China, in 1994, and MSc and PhD degrees in Geotechnical Engineering at Jilin University, China, in 1997 and 2001, respectively. She is professor of geotechnical engineering and deputy director of Department of Civil Engineering at Tianjin University. Dr. Lei has hosted a number of key projects from Chinese government, such as National Key Research and Development Program of China, National Key Basic Research and Development Program of China (973 Program), and National Natural Science Foundation of China. She has authored or co-authored more than 130 academic papers and compiled 9 tutorial books and monographs. Dr. Lei's research interests cover soft soil engineering characteristics, foundation treatment, soil constitutive relationship and urban underground engineering.